Applied Catalysis B: Environmental 334 (2023) 122872

Contents lists available at ScienceDirect

Applied Catalysis B: Environmental

journal homepage: www.elsevier.com/locate/apcatb

Unraveling alkali-tolerance role of zeolite coupling $CeWO_x$ catalyst for NO_x reduction

Gang Li [a,1], Yonglong Li [b,1], Dong Han [a], Wenming Liu [a], Meiyuan Liao [a], Lei Chen [b], Daishe Wu [b,c], Zhenguo Li [d], Linsheng Wei [b], Shengyong Lu [e], Honggen Peng [a,b,*]

[a] Key Laboratory of Jiangxi Province for Environment and Energy Catalysis, School of Chemistry and Chemical Engineering, Nanchang University, 999 Xuefu Road, Nanchang, Jiangxi 330031, China
[b] School of Resources and Environment, Key Laboratory of Poyang Lake Environment and Resource Utilization, Ministry of Education, Nanchang University, 999 Xuefu Road, Nanchang, Jiangxi 330031, China
[c] School of Materials and Chemical Engineering, Pingxiang University, Pingxiang, Jiangxi 33700, China
[d] National Engineering Laboratory for Mobile Source Emission Control Technology, China Automotive Technology & Research Center, Tianjin 300300, China
[e] State Key Laboratory for Clean Energy Utilization, Institute for Thermal Power Engineering, Zhejiang University, Hangzhou 310027, China

ARTICLE INFO

Keywords:
Nitrogen oxides
Ammonia selective catalytic reduction
Zeolite
$CeWO_x$
K-poisoning resistance

ABSTRACT

The deactivation of the selective catalytic reduction (SCR) catalysts in the presence of alkali metal is still unsolved to date, there is no fully effective strategy to remedy it. Herein, a series of novel zeolite coupling $CeWO_x$ catalysts ($CeWO_x$@ZSM-5) with core-shell structures was synthesized by a simple method. The proposed $CeWO_x$@ZSM-5 catalyst exhibited superior *de*NO_x performance and K-poisoning resistance, which are attributed to the synergy between the shell and active components. The zeolite shell with abundant acid sites can act as a sacrificial agent to preferentially bind to K, thereby decelerating/inhibiting the alkali metal poisoning process of the catalyst. Even after loading 1 wt% K, the NO_x conversion remained as high as > 80% at 300–500 °C over the $CeWO_x$@ZSM-5 catalyst under humid conditions. The novel zeolite coupling $CeWO_x$ catalyst may serve as a workable reference for new, efficient, and highly poisoning-resistant SCR catalysts for practical application.

1. Introduction

Nitrogen oxides (NO_x) generated by anthropogenic activity mainly originate from the combustion of fossil fuels, e.g., exhaust gas from car, diesel vehicles, and industrial kilns such as thermal power plants and cement plants [1–4]. The emission of large amounts of NO_x can lead to acid rain, photochemical smog, and haze that can severely impact the natural environment and human health [5–7]. Fortunately, NO_x can be effectively eliminated by selective catalytic reduction of NO_x with NH_3 (NH_3-SCR) technology, which is currently the most sophisticated and widely used technology to control NO_x emissions [8].

In the practical application of NH_3-SCR technology, the catalyst is the key part, and its performance directly affects the overall denitrification (*de*NO_x) efficiency and stability of the SCR system [9]. Its service life also determines the annual cost and process stability of SCR technology. However, *de*NO_x catalysts are generally deactivated after 24,000 h of operation. Frequent replacement of deactivated catalysts to satisfy *de*NO_x emission requirements is overly resource-consumptive [10]. The deactivation of catalysts is mainly divided into physical and chemical deactivation, and among the many factors of SCR catalyst deactivation, deactivation due to alkali and alkaline earth metals, e.g., [11–13] potassium (K), sodium (Na), calcium (Ca), and magnesium (Mg), is particularly significant [14,15].

For power plants and industrial boilers, commercial V_2O_5-$WO_3(MoO_3)/TiO_2$ catalysts are usually replaced or cleaned every 2–5 years. This is necessary mainly due to the cumulative deactivation of alkali metals present in the exhaust gas. The use of biomass fuels as a substitute for fossil fuels in some power plants and industrial boilers has resulted in higher alkali metal content in the flue gas and accelerated catalyst deactivation rates to 2–4 times higher than those in normal coal-fired power plants. Studies have shown that potassium is the main cause of catalyst deactivation at levels almost as high as 2 wt%. Alkali

* Corresponding author at: Key Laboratory of Jiangxi Province for Environment and Energy Catalysis, School of Chemistry and Chemical Engineering, Nanchang University, 999 Xuefu Road, Nanchang, Jiangxi 330031, China.
E-mail address: penghonggen@ncu.edu.cn (H. Peng).
[1] These authors contribute equally to this work.

https://doi.org/10.1016/j.apcatb.2023.122872
Received 10 December 2022; Received in revised form 6 May 2023; Accepted 8 May 2023
Available online 9 May 2023

poisoning remains a major obstacle to enhancing SCR catalyst performance at present [16,17]. Therefore, the development of SCR catalysts with significant resistance to alkali metal (K) poisoning has attracted a great deal of interest [18].

It has been reported that the reduced redox ability, surface acidity loss, and catalyst channel blockage are considered the primary deactivation factors in catalysts susceptible to alkali poisoning [19]. Several strategies have been put forward to improve the alkali resistance of SCR catalysts, such as supplying additional acid sites or using strongly acidic supports. Combining experiments and theoretical calculations, Peng et al. [20] demonstrated that the addition of CeO_2 to MnO_x/TiO_2 catalysts can improve the alkaline resistance over the catalysts; CeO_2 provides a new Lewis acid site for NH_3 adsorption and therefore maintains the catalyst reduction for NH_3 activation. Separating catalytically active sites and alkali-trapping sites within the catalyst system can also promote alkali resistance. For example, Zheng et al. [21] showed that V_2O_5/HWO catalysts have spatially separated catalytic active sites (CASs) and base trapping sites (ATSs). During the catalytic reaction, even if K^+ initially blocks CASs, ATSs spontaneously trap base ions such as K^+ thus releasing CASs and forming a self-protection mechanism against alkali poisoning.

In summary, the addition of additional acid centers can regulate the acidity of SCR catalysts. The separation of base trapping sites and active sites in the catalysts can hinder the direct contact between alkali metals and active sites, which can significantly improve the alkali resistance of catalysts [22,23].

The provision of additional acidic sites or the use of strongly acidic carriers to enhance the alkali resistance of catalysts has received widespread research attention. Alkali ions preferentially interact with the acidic carriers, thereby protecting the active sites. The application of $CeWO_x$ catalysts in NH_3-SCR reaction was first reported in the field of chemistry in 2011 [24]. In 2012, Peng et al. [25] found that CeO_2-WO_3 catalyst by introducing W has higher resistance to K-poisoning than V_2O_5-WO_3/TiO_2 catalyst. By separating the base-trapping and active sites in the catalysts, K can be preferentially trapped thus enhancing the anti-alkali metal poisoning ability of the catalyst. Although the CeO_2-WO_3 catalyst shows strong denitrification performance and a wide activity window, it is still inevitably poisoned and deactivated if exposed to alkali metals over time.

ZSM-5 zeolite is a classical NH_3-SCR catalyst support with abundant acidic sites, which gives it the potential to resist alkali poisoning [26,27]. In this study, a kind of zeolite coupling $CeWO_x$ ($CeWO_x$@ZSM-5) catalyst with core-shell confine structure was prepared with $CeWO_x$ binary metal oxides as the core and ZSM-5 as the shell. The proposed structure is shown to significantly improve the alkali metal poisoning resistance of the catalyst. To our knowledge, there have been few previous reports on improving alkali metal resistance via zeolite-metal oxides with core-shell confined structures.

2. Experimental materials and methods

2.1. Preparation of $CeWO_x$@ZSM-5 series catalysts

A one-pot two-step dry-gel conversion method was adopted to prepare zeolite coupling $CeWO_x$ (A% $CeWO_x$@ZSM-5, A=10, 15, 20, 25) catalysts with core-shell structures. The precursor $CeWO_x$@Al-SiO_2 was synthesized by reversed-phase microemulsion method, specifically, 960 mL of cyclohexane was added to a 2000 mL round bottom flask, 40.32 g of NP-5 (template agent) was weighed, and cerium nitrate and ammonium metatungstate (molar ratio 1:1) were dissolved in 4.32 mL of deionized water and added together to the round bottom flask. The resulting solution was stirred for 15 h at room temperature, then 4.32 mL of ammonia was added, and the stirring was continued for 2 h. 5 mL of tetraethoxysilane (TEOS) and 0.045 g of aluminum isopropoxide were added (where Si/Al = 100 for this catalyst), and the stirring was continued for 48 h. Finally, 500 mL of methanol was added to the solution to break the emulsion and left for 1 h, and then the lower floc was collected by centrifugation. A 1:1 mixture of cyclohexane and acetone was prepared to wash the lower floc. The precipitate was dried in an oven at 80 °C overnight to obtain the solid powder $CeWO_x$@Al-SiO_2, and then $CeWO_x$@ZSM-5 was synthesized by dry gel conversion. 0.200 g of $CeWO_x$@Al-SiO_2 and 0.266 g of tetrapropylammonium hydroxide (TPAOH) were weighed and ground in a mortar, and then dried under an infrared lamp for 15 min to remove the excess water. The dried powder was transferred to a high-pressure reaction kettle and placed in an oven at 80 °C for 48 h, 100 °C for 24 h, 120 °C for 24 h, and 150 °C for 24 h. Finally, the sample was roasted in a muffle furnace at 550 °C for 6 h in air atmosphere to remove the organic template agent and obtain the target catalyst, which was expressed as $CeWO_x$@ZSM-5.

For comparison, loaded catalysts and pure composite oxide catalysts, denoted as $CeWO_x$/ZSM-5 and $CeWO_x$, were prepared. According to the feeding molar ratio: 0.4TPAOH: 1.0SiO_2: 0.005Al_2O_3: 35H_2O. 13.8 g of TPAOH and 0.045 g of $NaAlO_2$ were added to 12.000 g of deionized water and stirred at room temperature until completely dissolved. TEOS was added to the above gel drop by drop and stirred vigorously for 6 h at room temperature, and the above gel was transferred to an autoclave and crystallized at 170 °C for 4 days in a homogeneous reaction chamber. After crystallization, the gel was naturally cooled to room temperature, then washed with deionized water to neutral and dried in an oven at 80 °C overnight. Finally, the dried solid powder was placed in a muffle furnace and roasted at 550 °C for 6 h to remove the template agent. The desired crude product, Na-ZSM-5, was obtained. Subsequently, Na-ZSM-5 was ion-exchanged with 0.1 mol L^{-1} NH_4Cl solution (1 g sample: 50 mL NH_4Cl solution) at 80 °C for 4 h and repeated three times to obtain NH_4-ZSM-5. Finally, NH_4-ZSM-5 was roasted in a muffle furnace at 550 °C for 4 h to obtain H-ZSM-5. Using the impregnation method, cerium nitrate and ammonium metatungstate were dissolved in 10 mL of distilled water at 1:1 molarity, and then 1 g of H-ZSM-5 was added to the solution and stirred for 4 h at room temperature, followed by evaporation of water by stirring in a water bath at 80 °C. The solid powder was dried in an oven for 12 h. Finally, the sample was roasted in a muffle furnace at 550 °C for 4 h under air atmosphere to obtain the comparison catalyst $CeWO_x$/ZSM-5. Cerium nitrate and ammonium metatungstate were dissolved in 100 mL of distilled water at 1:1 molarity, and then ammonia was added dropwise to pH = 10, and then washed with deionized water to neutral and dried in an oven at 80 ℃ overnight. Finally, the dried solid powder was placed in a muffle furnace and roasted at 550 °C for 4 h to obtain the comparison catalyst $CeWO_x$.

Alkali metal (K) poisoning treatment. 0.02 mol L^{-1} KNO_3 solution was mixed with freshly prepared catalyst, stirred at room temperature for 4 h, then placed in an oven at 80 °C and dried overnight and roasted at 550 °C for 4 h to obtain the poisoned catalysts. The loading of K in the catalysts was 1 wt%, which was expressed as 1% K-$CeWO_x$@ZSM-5, 1% K-$CeWO_x$/ZSM-5 and 1% K-$CeWO_x$.

Hydrothermal aging treatment. The catalysts were aged at 700 °C for 16 h. The aging unit consisted of a tube furnace, a mass flow meter and a bubbler. Pretreatment conditions: air, [H_2O] = 5 vol%, 16 h, 700 °C. The raw gas for hydrothermal aging was air 30 mL min^{-1}, and the samples were expressed as $CeWO_x$@ZSM-5-Aged, $CeWO_x$/ZSM-5-Aged and $CeWO_x$-Aged, respectively.

2.2. Catalytic performance tests

SCR activity was determined using a custom-built fixed-bed U-shaped quartz tube reactor (inner diameter = 6 mm) and 0.1 g catalyst. The gas mixture composition was [NO] = 500 ppm, [NH_3] = 500 ppm and [O_2] = [H_2O] = 5 vol%, and N_2 was the balance gas. The total flow rate was controlled to 100 mL min^{-1} corresponding to a gas hourly space velocity (WHSV) of 60,000 mL $g_{cat.}^{-1}$ h^{-1}. Gas concentrations were simultaneously monitored using Fourier transform infrared spectroscopy (FTIR) (Nicolet Antaris IGS Spectrometer). NO_x conversion and N_2 selectivity were calculated according the equal (1) and (2), respectively.

$$X_{NO_x} = \left(1 - \frac{[NO_x]_{out}}{[NO_x]_{in}}\right) \times 100\% \text{ with } [NO_x] = [NO] + [NO_2] \quad (1)$$

$$N_2 selectivity = \left(1 - \frac{2[N_2O]_{out}}{[NO_x]_{in} + [NH_3]_{in} - [NO_x]_{out} - [NH_3]_{out}}\right) \times 100\% \quad (2)$$

where NO_x denotes the total concentration of NO and NO_2. $[N_2O]_{out}$, $[NO_x]_{in}$, $[NO_x]_{out}$, $[NH_3]_{in}$, and $[NH_3]_{out}$ indicate the corresponding inlet and outlet gas concentrations. A more detailed description of the catalytic performance measurements is given in the Supporting Information section.

Kinetics were observed in the kinetic region in differential reaction mode with NO_x conversion of less than 15%, and were also performed under the humid conditions. The gas mixture composition was [NO] = 500 ppm, $[NH_3]$ = 500 ppm and $[O_2] = [H_2O]$ = 5 vol%, and N_2 was the balance gas. The total flow rate increased to 400 mL min^{-1}, 0.025 g of catalyst and 0.075 g of quartz sand weighed and mixed, thus the WHSV was 960,000 mL $g_{cat.}^{-1}$ h^{-1}. The absence of mass and heat transfer limitations was verified, including the Mears criterion (C_M) for external diffusion, the Weisz-Prater criterion (C_{WP}) for internal diffusion, and the Mears criterion ($C_{Me.}$) for heat transfer (Supporting Information).

2.3. Characterization

X-ray diffractometer (SmartLab9KW) is used to analyze the physical phase structure of the sample. The morphology and elemental dispersion of the catalysts were characterized on transmission electron microscope (TEM) and EDX mapping images. The BET surface areas and pore volumes of the catalysts were measured by nitrogen ad-sorption–desorption obtain N_2 adsorption and desorption isotherms using an Kubo-X1000 specific surface area analyzer at − 196 °C. The chemical properties of the samples were characterized using various measurement methods including PCA-1200 chemisorption analysis. The test steps are as follows: The amount of catalyst was 80 mg. The samples were pretreated for 60 min at 300 °C under Ar atmosphere and then cooled to room temperature. The pretreatment gas was changed to 10% H_2/Ar mixture, and after the baseline stabilized, the programmed ramp-up program was set to increase the sample bed from room temperature to 1000 °C at a ramp-up rate of 10 °C min^{-1}. The corresponding test signals were detected by a thermal conductivity detector (TCD) and the experimental results were recorded. A laser Raman spectrometer from Renishaw Ltd, UK was used. The samples were pressed and swept for spectra in the range of 200–1200 cm^{-1}. X-ray photoelectron spectroscopy (XPS) (PHI 5000 CESCA System), the XPS date from the regions related to the Ce 3d, W 4f, O 1s were recorded. The binding energies were calibrated internally by the carbon deposit C 1 s binding energy at 284.8 eV. NH_3 programmed temperature rise desorption (NH_3-TPD) was measured by Micromeritics ASAP 2920 with a TCD detector. After pretreatment purging the samples at 400 °C for 1 h in pure Ar, the samples were cooled down to 50 °C and NH_3 adsorption was performed at 50 °C for 1 h, followed by purging with Ar. Finally, the samples were heated from 50 °C to 700 °C at a heating rate of 10 °C min^{-1}. In situ DRIFTS spectra were recorded on a Bruker Vertex spectrometer with a mercury cadmium telluride (MCT) detector cooled with liquid nitrogen. Prior to the experiment, the samples were pretreated in N_2 at 400 °C for an hour. Background spectra were collected in the N_2 atmosphere and automatically subtracted from the sample spectra. Sixty IR spectra were recorded by 1 min/scan at a spectral resolution of 4 cm^{-1}.

3. Results and discussion

3.1. NH_3-SCR performance evaluation of catalysts

Since H_2O cannot be avoided during the SCR process due to the presence of a certain amount of water in exhaust, therefore, all the activity tests were measured under the wet reaction conditions with 5 vol % H_2O. First, the activity of $CeWO_x$@ZSM-5 series of catalysts with different $CeWO_x$ contents was tested, and the results are shown in (Figs. 1a, S1). The temperature window of the catalyst grew wider and low temperature activity was enhanced as $CeWO_x$ content increased; there was no further improvement in catalytic activity once the $CeWO_x$ content exceeded 20%. The 15% $CeWO_x$@ZSM-5 catalyst showed the optimal SCR activity among the catalysts we tested, so we used the 15% $CeWO_x$@ZSM-5 catalyst (referred to from here on as simply "$CeWO_x$@ZSM-5") for all subsequent analyses.

Fig. 1b shows the NO_x conversion of fresh $CeWO_x$@ZSM-5, $CeWO_x$/ZSM-5 and $CeWO_x$ catalysts and pure ZSM-5 zeolite. $CeWO_x$@ZSM-5, $CeWO_x$/ZSM-5 and $CeWO_x$ catalyst all maintain an excellent NO_x conversion temperature window, while pure ZSM-5 molecular sieves have almost no activity, with $CeWO_x$@ZSM-5 and $CeWO_x$/ZSM-5 catalysts achieving 90% NO_x conversion at 500 °C. It appears that the composite of zeolite and metal oxide significantly improved the high temperature activity of the catalyst. When the reaction temperature exceeded 500 °C, a slight decrease in high temperature SCR activity was observed due to NH_3 oxidation [28]. However, 99% N_2 selectivity was maintained in the range of 240–550 °C and the concentration of by-product N_2O were consistently below 5 ppm (Fig. S2).

Kinetic analysis data were derived from intrinsic kinetic tests conducted at high WHSV (960,000 mL $g_{cat.}^{-1}$ h^{-1}) for excluding heat transfer limitations (Supporting Information). The NO_x conversions below 15% were selected to exclude the effect of internal diffusion. The Arrhenius plots and apparent activation energy (E_a) values of the two samples are shown in (Fig. S3) and (Table S1). The E_a of $CeWO_x$@ZSM-5 and $CeWO_x$/ZSM-5 were 63 and 77 kJ mol^{-1}, respectively. To this effect, a relatively E_a favors the NH_3- SCR reaction.

In practical applications, there are other components in flue gas that affect the performance of catalyst. For the catalytic purification of exhaust gases such as in coal-fired power plants, alkali metal poisoning is a serious problem. After 1 wt% K poisoning of fresh catalysts, as shown in (Fig. 1c), the activity-temperature curves of $CeWO_x$@ZSM-5 and related catalysts before and after K poisoning show that the performance of 1% K-$CeWO_x$@ZSM-5 catalyst slowly decreased, but the NO_x conversion was still more than 80% within the 300–500 °C and with low concentrations of N_2O by-products (Fig. S4). The 1% K-$CeWO_x$/ZSM-5 catalyst was only able to remove > 80% of NO_x from the simulated exhaust gas at 400–500 °C. However, the 1% K-$CeWO_x$ composite metal oxide catalyst, lost most denitrification activity under the same K-poisoning treatment conditions. The novel zeolite coupling metal oxide catalyst ($CeWO_x$@ZSM-5) thus shows better alkali metal (K) resistance than the $CeWO_x$/ZSM-5 or $CeWO_x$ composite metal oxide catalysts.

The catalyst stability during the NH_3-SCR reaction is also relevant to the industrial application of the catalyst, which includes high-temperature hydrothermal stability for high-temperature thermal effects [29,30]. The catalysts were hydrothermally aged at 5% H_2O/Air at 700 °C for 16 h to test these qualities. The corresponding aged catalysts are denoted by the suffix-Aged (e.g., $CeWO_x$@ZSM-5-Aged). The low-temperature activity (<300 °C) of the hydrothermal-aged catalyst $CeWO_x$@ZSM-5-Aged decreased slightly, but there was no significant effect on the high-temperature activity (Fig. 1d). By contrast, the catalysts $CeWO_x$/ZSM-5-Aged and $CeWO_x$-Aged showed a very obvious decrease in low-temperature activity after hydrothermal aging treatment and a slight decrease in high-temperature activity. Besides, the catalysts after hydrothermal treatment also showed excellent N_2 selectivity and low N_2O by-product concentration (Fig. S5).

Combining the XRD (Fig. S6) and adsorption-desorption curves (Fig. S7) of the catalysts before and after aging with the specific surface area data (Table S2) shows that the crystallinity and specific surface area of all the aged catalysts decreased. $CeWO_x$/ZSM-5-Aged and $CeWO_x$-Aged catalysts showed a significant enhancement in the characteristic diffraction peaks of CeO_2, while the $CeWO_x$@ZSM-5-Aged catalyst showed no significant change. It indicates that the core-shell structure can stabilize the Ce-W active component and prevent the metal oxides

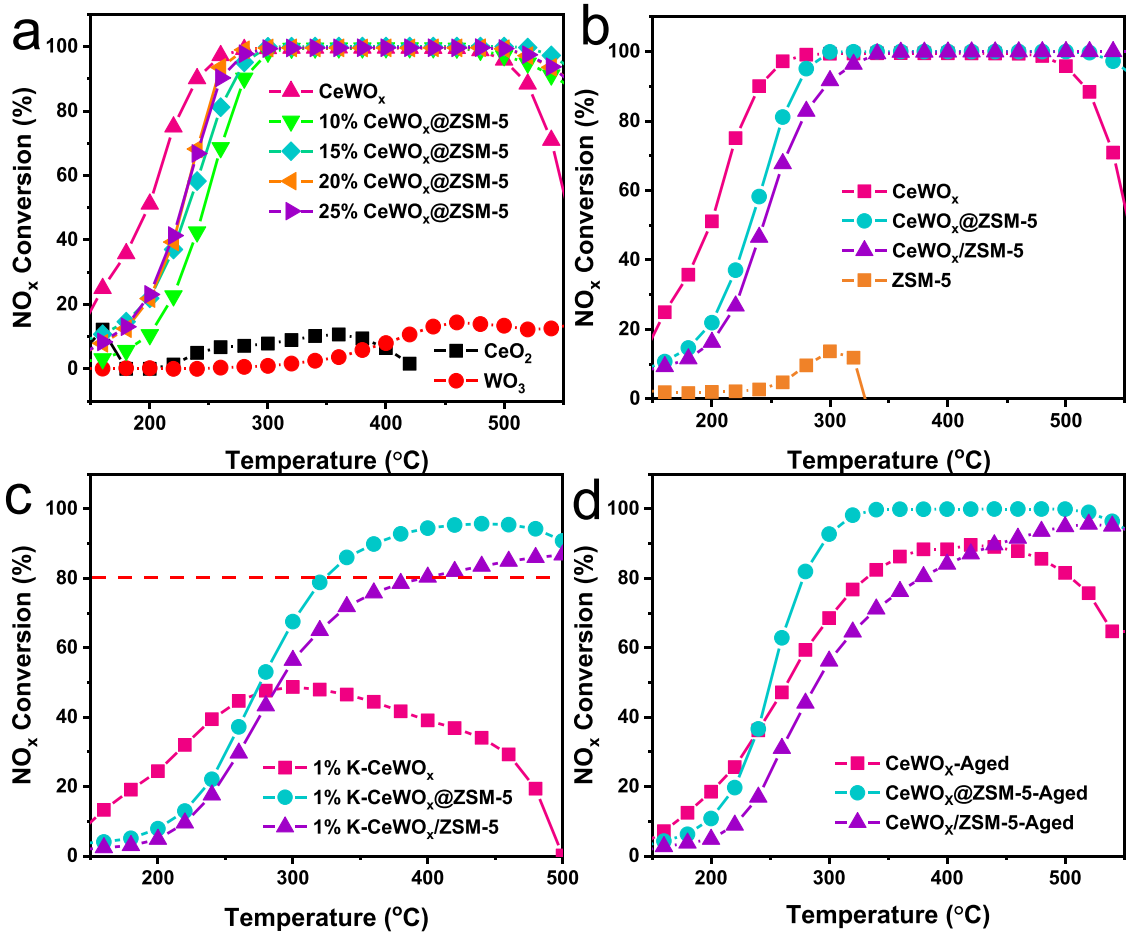

Fig. 1. (a) NO_x reduction activity of $CeWO_x$@ZSM-5 catalysts with different $CeWO_x$ content; (b) NO_x reduction activity of $CeWO_x$@ZSM5 and comparative catalysts; (c) Catalytic activity after K poisoning; (d) High-temperature hydrothermal aging performance test, pre-treatment conditions: Air, [H_2O] vol%, 16 h, 700 °C. Reaction conditions: [NO] = [NH_3] = 500 ppm, [O_2] = [H_2O] = 5 vol% (when used), N_2 balance, WHSV = 60,000 mL $g_{cat.}^{-1}$ h^{-1}.

from sintering at high temperatures, which is beneficial to the stability of the active component [31].

Besides, the deactivation caused by water is mainly due to the competition of water with NH_3 and NO for adsorption to grab the active site [32], and the H_2O often have negligible impact on the *de*NO_x catalysts at high temperatures (> 300 °C), so the catalysts were tested for long-term water resistance at lower temperature at 240 °C. In this work, after the activity test, the catalyst was stabilized at 240 °C for 1 h, the water vapor was withdrawn after 10 h of continuous reaction by passing 5% H_2O for additional 1 h. From Fig. 2a, the activity of the $CeWO_x$@ZSM-5 catalyst decreased by 17% after passing water vapor; the activity recovered rapidly to nearly the initial level after the withdrawal of water vapor. The activity of the $CeWO_x$/ZSM-5 catalyst decreased by 27% after the introduction of water vapor; the activity also recovered rapidly after withdrawing the water vapor but did not fully recover to the initial activity. This indicates that the hydrophobic molecular sieve core-shell structure has more excellent water resistance.

Similarly, SO_2 is a gas commonly emitted from coal-fired boilers and one of the species that tend to poison the SCR denitrification catalyst in boilers. SO_2 is easily oxidized to SO_3 by the catalyst [33,34]. It reacts with water and NH_3 in the flue gas to form ammonium sulfate (AS) and ammonium bisulfate (ABS), which are deposited on the catalyst surface affecting its activity [35]. SCR activity tests were performed with 50 ppm SO_2 in the reaction feed gas (Figs. 2b, S8) and sulfur resistance (300 °C, [SO_2] = 50 ppm, [H_2O] = 5 vol%, 10 h) conditions (Fig. 2c). The $CeWO_x$ metal oxide catalyst itself showed excellent water and sulfur resistance. The $CeWO_x$@ZSM-5 catalyst shows strong and sustained resistance to SO_2 poisoning.

3.2. Morphologies and structures of catalysts

The physical phase structure of the as-prepared catalysts was analyzed by X-ray diffraction (XRD). The prepared $CeWO_x$ composite metal oxides showed obvious characteristic peaks of CeO_2 and WO_3. The precursor $CeWO_x$@Al-SiO_2 showed stronger characteristic peaks of CeO_2 with increasing loading of the composite metal oxides (Fig. S9) and $CeWO_x$@ZSM-5 with varying amount of cerium and tungsten prepared by converting the amorphous Al-SiO_2 shell layer into molecular sieve shell layer via dry-gel conversion method. Molecular sieve coupling catalysts all showed characteristic diffraction peaks at the typical MFI structure, indicating the successful synthesis of $CeWO_x$@ZSM-5 (Fig. S10). The characteristic diffraction peak of CeO_2 was detected at 28.8° for the zeolite with different contents of $CeWO_x$@ZSM-5 [36]. The peak intensity at 28.8° increased significantly as the amount of wrapped metal oxides increased, while there was no characteristic diffraction peak of WO_3; presumably, W was highly dispersed in the molecular sieve. A slight enhancement of the peak intensity of the characteristic diffraction peak of CeO_2 at 28.8° for the 1% K-$CeWO_x$@ZSM-5 catalyst was observed after K-poisoning. For the 1% K-$CeWO_x$/ZSM-5 catalyst, the peak intensity of the characteristic diffraction peak of CeO_2 located at 28.8° was significantly enhanced (Fig. S11). Both, however, still showed the characteristic peaks of the intact MFI crystalline form, which proves that K caused the Ce species aggregation. The $CeWO_x$@ZSM-5 catalyst hindered the aggregation of Ce species due to the shielding

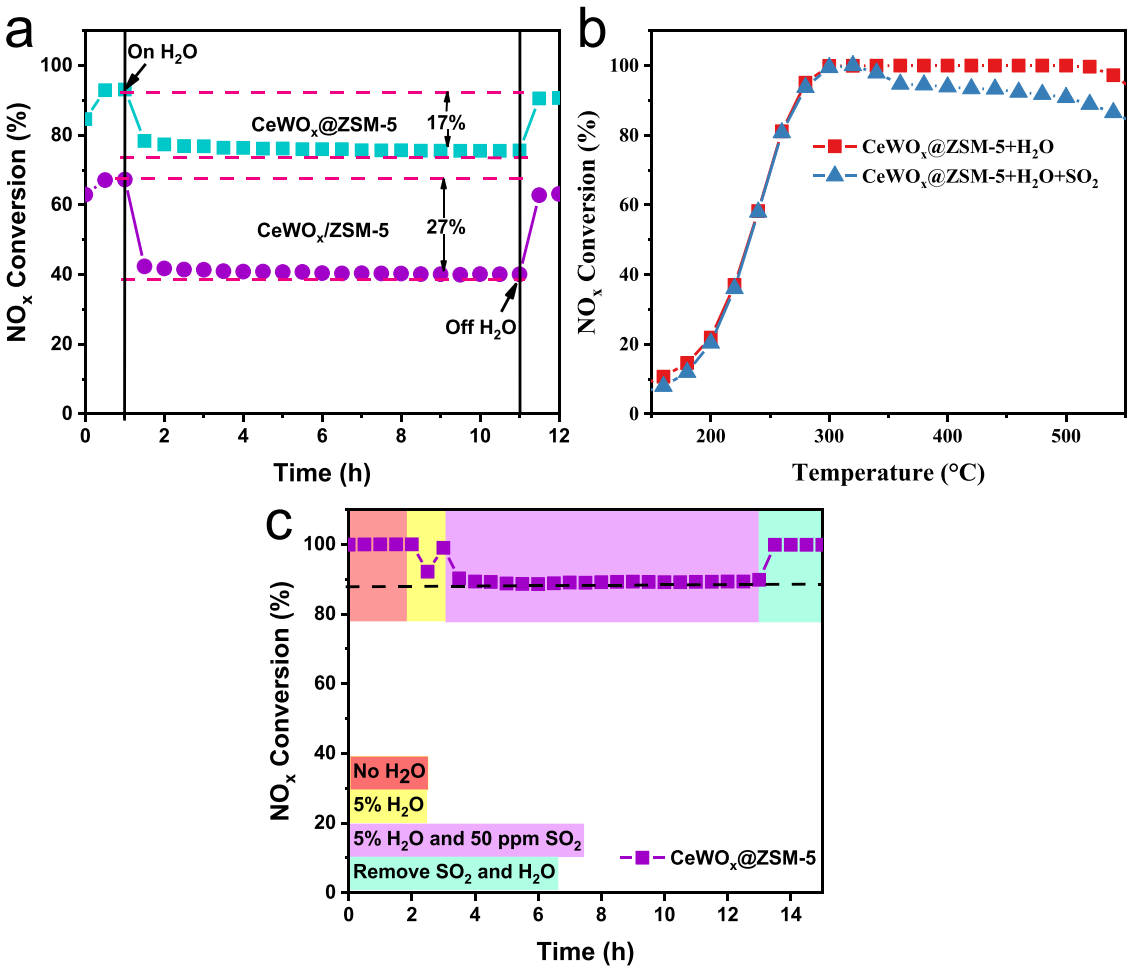

Fig. 2. (a) Water resistance test at 240 °C; (b) NO_x conversion as a function of temperature in NH_3-SCR reaction over the catalysts of $CeWO_x$@ZSM-5; (c) $CeWO_x$@ZSM-5 catalyst tested for long-term water and sulfur resistance at 300 °C. Reaction conditions: [NO] = [NH_3] = 500 ppm, [O_2] = [H_2O] = 5 vol% (when used), N_2 balance, WHSV = 60,000 mL $g_{cat.}^{-1}$ h^{-1}.

effect of its core-shell structure.

The N_2 adsorption-desorption isotherm plots (Fig. S12) show that all the above catalysts have type I adsorption-desorption isotherms, but the core-shell catalysts prepared by the dry-gel conversion method all show H3-type hysteresis loops, indicating the existence of mesopores in the catalysts prepared by this method. The mesopore pore size was mainly at 3.66 nm as per the pore size distribution of the main catalyst (Fig. S13).

Table S2 shows the specific surface area and pore volume obtained by N_2 adsorption-desorption test results. The specific surface area appears to decrease regularly as active component loading increases (Table S3). However, the specific surface area of the 1% K-$CeWO_x$ @ZSM-5 catalyst decreased significantly after K poisoning, from 388 m^2 g^{-1} in fresh to 340 m^2 g^{-1}. This occurred mainly due to the deposition of K_2O, which collected on the catalyst surface and blocked its pores. The pore volumes of the catalysts after poisoning were all reduced compared to the fresh catalysts, indicating that the toxic substances penetrated the pore channels of the zeolite material.

TEM results showing the structures and morphologies of the fresh $CeWO_x$@ZSM-5 and related catalyst samples are shown in Fig. 3. Compared to the loaded $CeWO_x$/ZSM-5, the outer layer of the core-shell $CeWO_x$@ZSM-5 catalyst shows no obvious particle buildup. Active component particles can be clearly observed in both samples (Fig. 3a-d) as metal oxides belonging to CeO_2 and WO_3 [37,38]. Comparing the $CeWO_x$@ZSM-5 and $CeWO_x$/ZSM-5 catalysts EDS-mapping (Fig. S14), it was found that the Ce, W dispersion on the $CeWO_x$@ZSM-5 catalyst was higher and uniformly dispersed on the carrier as well as being encapsulated inside the carrier. Furthermore, the $CeWO_x$@ZSM-5 catalyst showed a significant aggregation of Ce species on the surface, with most of the metal oxide particles distributed on the carrier.

The active components are encapsulated in zeolite shell layer which is difficult to distinguish. To further demonstrate the formation of the core-shell structure, the samples were pretreated by resin-embedded ultrathin sectioning and cut into ultrathin sections of a certain nanometer thickness, thereby performing TEM characterization X-ray energy spectrometry (EDS) analysis of the cross section of the catalyst body. HADDF-TEM images show (Fig. 3e, f) that the active components are clearly wrapped inside the molecular sieve shell layer from the cut section of the catalyst. EDS-mapping results (Fig. 3g-l) also show that Ce and W elements are uniformly wrapped inside the ZSM-5 zeolite, with Si and Al elements are distributed throughout the catalyst particles. These results further confirm the integrity of the core-shell structure of the catalyst.

3.3. Catalyst-related chemical characterization

3.3.1. Redox performance analysis of catalysts

The redox performance of the catalyst is another important performance indicator. The redox properties of the samples were characterized by using the H_2 programmed warming reduction method, as shown in (Fig. 4a). In the fresh catalyst, the peaks located at low temperatures of 335, 432, 514 °C can be attributed to the reduction of surface oxygen (Ce^{4+}→Ce^{3+}); the peak at 890 °C is attributable to the reduction peak of

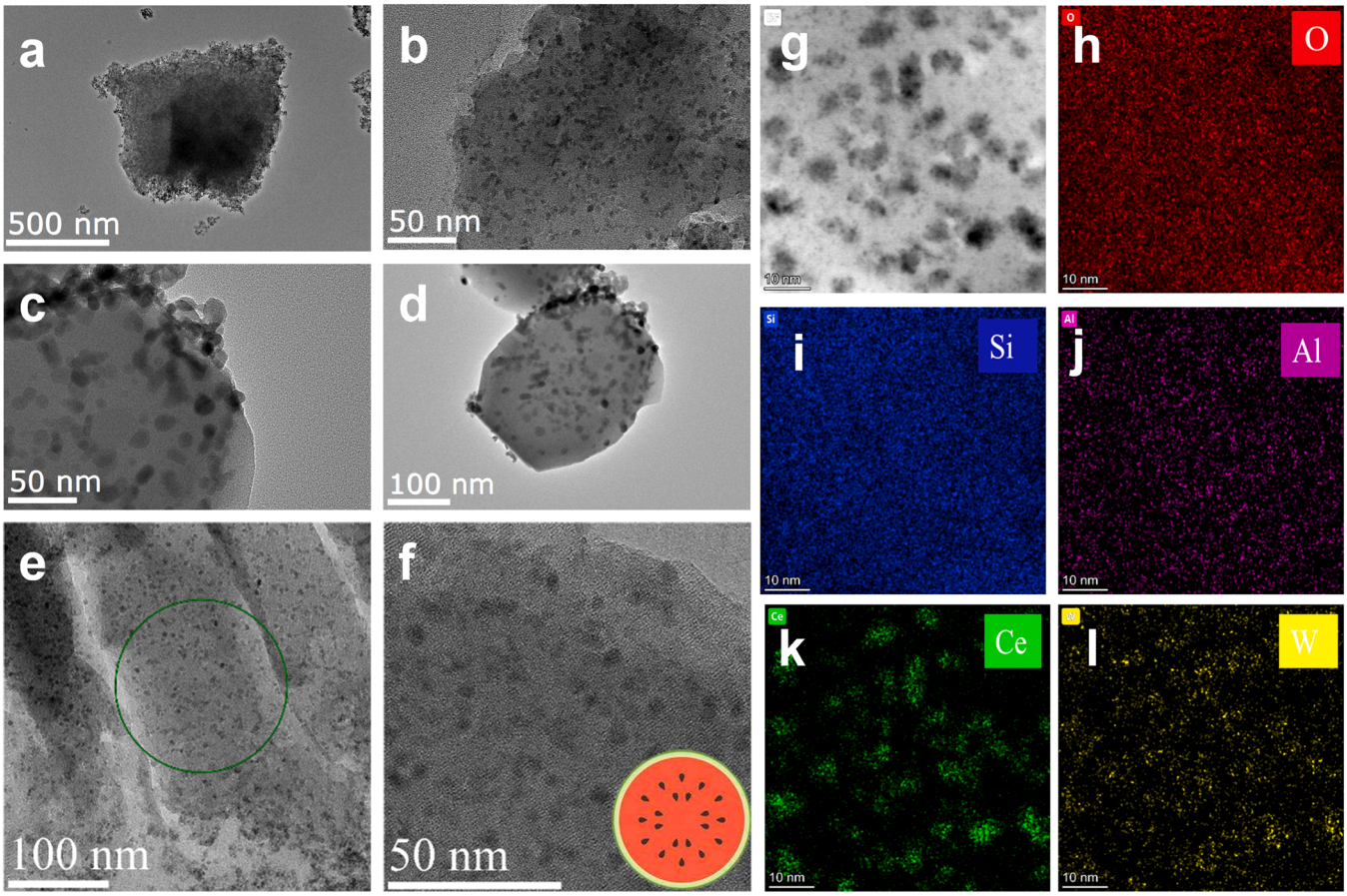

Fig. 3. TEM images of $CeWO_x$@ZSM-5 (a, b) and $CeWO_x$/ZSM-5 (c, d); HADDF-TEM of $CeWO_x$@ZSM-5 (e, f); EDS-Mapping images (g-l) of $CeWO_x$@ZSM-5.

bulk phase oxygen (Ce^{4+}→Ce^{3+}) [39,40]. 719 °C to the reduction peak of W (W^{6+}→W^0), and the peaks at 635, 921 °C to the overlap of Ce and W ions in the bulk phase reduction peaks. The reduction peak temperatures of the core-shell $CeWO_x$@ZSM-5 catalysts appear to be slightly higher than those of the loaded $CeWO_x$/ZSM-5 catalysts, which may be been caused by the shielding effect of the shell layer. However, the redox ability of the catalysts is not only related to the peak position but also to the peak intensity and peak area. On the $CeWO_x$@ZSM-5 catalyst, the peak area of surface oxygen reduction (Ce^{4+}→Ce^{3+}) is significantly larger than that of the $CeWO_x$/ZSM-5 catalyst, highlighting the high dispersion of Ce species in the $CeWO_x$@ZSM-5 catalyst [41]. In general, the reduction of hydrogen starts with the contact of surface oxygen and after some time, the oxide particles are completely covered by a layer of metal products formed in the reduction reaction, which inhibits the reduction of large metal oxides. Therefore, highly dispersed metal oxides of small particle size contribute to enhancing this reduction [42]. It is reported that there are two kinds of oxygen storage sites on the surface and subsurface of cerium-based catalysts, which exhibit different oxygen storage processes under different reaction conditions and may affect the catalytic performance [43]. For the poisoned catalysts, the reduction peaks of Ce species weakened in intensity and the initial consumption point of H_2 moved to a higher temperature, showing the same trend of movement as the NH_3-SCR performance. In addition, the reduction peak of W species also shifted to higher temperatures, indicating a loss of reduction of tungsten oxide as well.

3.3.2. *Raman spectroscopy of catalysts*

To further characterize the state of active components Ce and W on the catalysts, Raman tests were performed before and after poisoning as shown in (Fig. 4b). All Raman spectra were corrected by the peak at 520.5 cm^{-1}. Among them, the peak at 464 cm^{-1} corresponds to the $F_{2\,g}$ mode of the symmetric breathing mode of the oxygen atom around the cerium ion in the cubic fluorite phase CeO_2 [44], 810 cm^{-1} is attributed to the W-O stretching $A_{1\,g}$ mode, and 383 and 960 cm^{-1} are attributed to the $WO_{2(t)}$ stretching mode of the heteropolitungstate species [45,46]. The intensity of the peak of $CeWO_x$@ZSM-5 is significantly weaker than that of $CeWO_x$/ZSM-5, indicating that most of the Ce and W species were encapsulated inside the ZSM-5 shell layer. There is a weak enhancement of the peak located at 464 cm^{-1} in the 1% K-$CeWO_x$/ZSM-5 catalyst, presumably caused by the aggregation of K and Ce due to the interaction; this is consistent with the XRD results. The peak at 930 cm^{-1} shows significant weakening, which is mainly due to the interaction between K and tungstate species having decreased its surface acidity. The intensity of the diffraction peak of the 1% K-$CeWO_x$@ZSM-5 catalyst did not change significantly, however, presumably due to the shielding effect of the ZSM-5 shell layer on the active component which may have prevented it from direct contact with K.

3.3.3. *Analysis of NH_3-TPD results for catalysts*

Many researchers have shown that K poisoning decreases the number and strength of acidic sites in catalysts. The method focuses on the resistance of the molecular sieve shell layer to the alkali metal (K) poisoning of catalysts. The ammonia programmed temperature rise curves of the fresh and post-poisoning $CeWO_x$@ZSM-5 and related catalysts to quantify the acid sites on the catalyst surface. Fig. 4c shows the ammonia profiles of fresh $CeWO_x$@ZSM-5, $CeWO_x$/ZSM-5, $CeWO_x$ catalysts and post-K poisoning 1% K-$CeWO_x$@ZSM-5, 1% K-$CeWO_x$/ZSM-5, 1% K-$CeWO_x$ ammonia programmed ramp-up desorption curves for 1% K-$CeWO_x$ catalysts. The fresh catalysts show two desorption peaks at 100 °C and around 300 °C corresponding to the desorption of weakly adsorbed NH_3 and strongly adsorbed NH_3 [47], respectively. The NH_3 desorption peak at about 300 °C on the catalyst after K poisoning almost

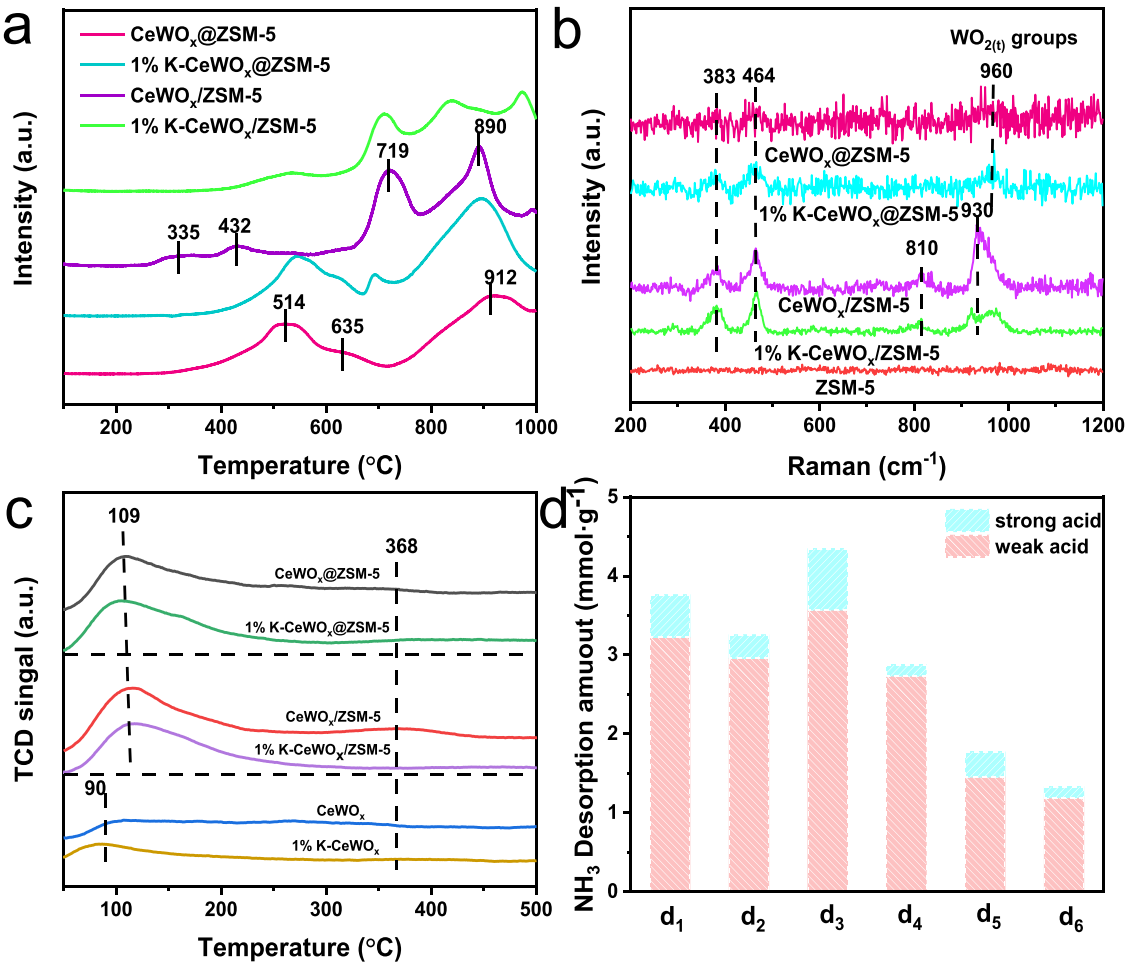

Fig. 4. (a) H_2-TPR profiles of $CeWO_x$@ZSM-5, $CeWO_x$/ZSM-5, 1% K-$CeWO_x$@ZSM-5 and 1% K-$CeWO_x$/ZSM-5 catalysts; (b) Raman spectra of $CeWO_x$@ZSM-5, $CeWO_x$/ZSM-5, 1% K-$CeWO_x$@ZSM-5, 1% K-$CeWO_x$/ZSM-5 and ZSM-5 catalysts; (c) NH_3-TPD profiles of the fresh and poisoned catalysts; (d) Acid amounts calculated from NH_3-TPD of fresh and poisoned catalysts: $CeWO_x$@ZSM-5(d_1), 1% K-$CeWO_x$@ZSM-5(d_2), $CeWO_x$/ZSM-5(d_3), 1% K-$CeWO_x$/ZSM-5(d_4), $CeWO_x$ (d_5), 1% K-$CeWO_x$ (d_6) of all catalysts.

disappeared, which should be the strong acid on ZSM-5, and main acid sites below 300 °C were retained to facilitate the adsorption and activation of NH_3 on 1% K-$CeWO_x$@ZSM-5 catalyst.

From the results of the quantitative analysis (Fig. 4d and Table S4), it can be concluded that the total NH_3 desorption of both core-shell and loaded catalysts was significantly larger than that of the pure oxide catalyst, indicating that the ZSM-5 was also equally acidic, which improved the adsorption of NH_3 onto the target catalyst. The total desorption of NH_3 from all poisoned catalysts showed a significant reduction, with the smallest reduction in 1% K-$CeWO_x$@ZSM-5. The NH_3 desorption and the total desorption of ammonia decreased from 3.76 to 3.27 mmol g^{-1}, while the total desorption of 1% K-$CeWO_x$/ZSM-5 decreased from 4.02 to 2.3 mmol g^{-1}, indicating that the core-shell structure effectively decelerated loss of the acid sites of the catalyst allowing it to retain excellent NH_3 adsorption capacity. The amount of acid sites on the catalyst surface plays an important role in the NH_3-SCR reaction system [48–50]; this is also consistent with the activity test results of the catalyst before and after poisoning.

3.3.4. *Valence analysis of surface elements of catalysts*

In this work, XPS technology was performed to investigate the presence of active components on the surfaces of $CeWO_x$@ZSM-5 and $CeWO_x$/ZSM-5 catalysts. Figs. S15–S17 shows the XPS spectra of Ce 3d, W 4f, and O 1s on $CeWO_x$@ZSM-5 and $CeWO_x$/ZSM-5 with absorption peaks calibrated on the C 1s peak at 284.6 eV. Fig. S15 shows the Ce 3d spectrum of the catalyst in question; the peaks labeled u`, v` on the spectrum indicate the initial electronic state of Ce^{3+} on $3d^{10}4f$.

[1] while the peaks labeled u, u``, u``, v, v``, and v``` on the spectrum indicate the initial electronic state of Ce^{4+} on $3d^{10}$. Their calculation shows that the $Ce^{3+}/(Ce^{4+}+Ce^{3+})$ ratio of $CeWO_x$@ZSM-5 (29.5%) was slightly higher than $CeWO_x$/ZSM-5 (29.2%). The presence of Ce^{3+} may lead to charge imbalance and unsaturated chemical bonding on the sample surface, thus improving the amount of chemisorbed oxygen on the catalyst surface [51–53]. The increase in chemisorbed oxygen facilitates the SCR reaction.

Fig. S16 shows the spectrogram of W 4f of the catalyst, revealing two main peaks in the binding energy range from 32 to 48 eV, which are in agreement with the peak positions of W 4 $f_{7/2}$ and W 4 $f_{5/2}$ of the pure oxide WO_3 and indicate the 7/2 and 5/2 spin orbitals of W corresponding to W^{6+}. Thus, W was present in the + 6 valence form in both catalysts and the oxidation state of W did not change [54,55]. The W 4f spectrum of the $CeWO_x$/ZSM-5 catalyst also shows a single line state loss characteristic peak centered at 39.9 eV. Combined with the O 1s spectra of (Fig. S17), the fitted peaks correspond to chemisorbed oxygen (O_α) and lattice oxygen (O_β), respectively, with peaks at binding energies of 531.0–533.0 eV assigned to O_α) and peaks at lower binding energies of 529.0–531.0 eV for surface lattice oxygen (O_β) [56,57]. The same calculation for its O_α content yielded a significantly larger chemisorbed oxygen content for $CeWO_x$@ZSM-5 (96.2%) than for $CeWO_x$/ZSM-5 (81.3%). Generally, chemisorbed oxygen is more reactive than lattice oxygen, has higher reaction mobility, and has a significant contribution to SCR activity [58], as evidenced by the above SCR catalytic test results.

Combining all the spectra, the results show a significant difference in peak signal intensities between $CeWO_x$@ZSM-5 and $CeWO_x$/ZSM-5. The Ce 3d and W 4f spectra of the $CeWO_x$@ZSM-5 catalyst have significantly weaker signal intensities than $CeWO_x$/ZSM-5. This is mainly due to the detection limit of XPS and is a side effect of the fact that a large amount of Ce and W active components are encapsulated in the ZSM-5 zeolite.

3.4. Reaction mechanism

3.4.1. In-situ DRIFTS

Both pretreatment and background acquisition were performed prior to the experiments in the following steps. First, $CeWO_x$@ZSM-5 and $CeWO_x$/ZSM-5 catalysts were treated with N_2 at 400 °C for 1 h. CO_2 and H_2O were blown out of the pipeline, cooled to the target temperature of 250 °C, and the background spectra were measured under a N_2 atmosphere. NH_3 (15 mL min^{-1}, N_2 as equilibrium gas) was passed at this temperature for 60 min while the in-situ DRIFT spectra were recorded starting in time steps. The results are shown in Fig. 5a, b.

For $CeWO_x$@ZSM-5 and $CeWO_x$/ZSM-5 catalysts, the peaks at 3689 and 3600 cm^{-1} are attributable to the vibrational peaks of Si-OH and Si-(OH)-Al, respectively, which belong to the Brønsted acid sites of them [59]. NH_4^+ is the main product of NH_3 adsorption on the surface of the H-type molecular sieve. NH_3 adsorption on the L-acid site and NH_3 adsorption on the B-acid site of the molecular sieve surface generate NH_4^+ to compensate for the negative charge on molecular sieve skeleton surface, a process that consumes the surface hydroxyl groups [60]. Therefore, after 10 min of NH_3 adsorption, an inverted peak appeared at 3600 cm^{-1}. The main peaks (3361, 3274 and 3183 cm^{-1}) were found at 3400–3000 cm^{-1} [61,62], associated with N-H bond stretching vibrations, and the bands at 3361 and 3274 cm^{-1} are attributed to the NH_4^+ ions, while the band at 3183 cm^{-1} can be attributed to coordinated NH_3. 1460, 1641 and 1169 cm^{-1} can be attributed to the deformation of NH_4^+ adsorbed on the protonic acid site and the vibration of the L acid site, respectively. Vibrations and symmetric vibrations occurred in adsorbed NH_3 on the L-acid site [63,64]. The 1530 cm^{-1} peak may be associated with intermediates of ammonia oxidation attributed to -NH_2 species. Compared to Fig. 5b1, Fig. 5a1 shows that the peak intensity of the $CeWO_x$@ZSM-5 catalyst was slightly weaker than that of the $CeWO_x$/ZSM-5 catalyst, indicating that the $CeWO_x$@ZSM-5 catalyst had fewer NH_3 adsorption sites than the $CeWO_x$/ZSM-5 catalyst. These results are in accordance with the NH_3-TPD results.

After saturation of its NH_3 adsorption, NH_3 was turned off, purged for 1 h, and the spectrum was detected. NO+O_2 (15 mL min^{-1}, N_2 as the equilibrium gas) was introduced while the in-situ DRIFT spectra were recorded in time steps. Fig. 5c, c1, d, d1 showed the spectra of $CeWO_x$@ZSM-5 and $CeWO_x$/ZSM-5 catalysts adsorbed with saturated NH_3 at 250 °C after the passage of NO + O_2, indicating the variation of adsorbed species with time. The adsorption products of NH_3 reacted rapidly with NO and O_2, and the intensity of the characteristic peaks of NH_3 adsorption products in the spectra diminished rapidly until disappearing within 5 min. Only weak Lewis acid (1191 cm^{-1}) was present at the fifth minute while weak NO_2 appeared (1625 cm^{-1}). Ten minutes later, the catalyst surface was rapidly covered by nitrate species (1692 cm^{-1}, 1625 cm^{-1}, 1511 cm^{-1}, 1173 cm^{-1}) [65] and the peak intensities did not change significantly, indicating that the adsorbed NO_x species may be non-active. Among them, the peak at 1625 cm^{-1} is attributable to the NO_3^- featured peak (bridging nitrate) which originated from NO_2 adsorbed on the oxide surface. The peak at 1511 cm^{-1} can be attributed to the asymmetric NO_2 vibration of bidentate nitrate and the peak at 1173 cm^{-1} to the symmetric NO_2 vibration of monodentate nitrite. These results indicate that the NH_3 species in the adsorbed state on the surface of $CeWO_x$@ZSM-5 and $CeWO_x$/ZSM-5 catalysts reacted with gas-phase NO + O_2, thus, followed the E-R mechanism.

To further investigate the adsorption of NO_x on the catalyst, a transient adsorption of NO + O_2 followed by NH_3 was carried out. The $CeWO_x$@ZSM-5 catalyst was pretreated as shown above, then the physically adsorbed NO + O_2 was purged with N_2 after passing NO + O_2 for 60 min at 250 °C followed by NH_3 adsorption. As shown in Fig. S18, the peaks at 1059 and 1120 cm^{-1} can be attributed to the asymmetric and symmetric NO vibrations of monodentate nitrate, respectively; the characteristic peaks at 1542 and 1240 cm^{-1} are attributable to the asymmetric and symmetric NO_2 vibrations of bidentate nitrate, respectively. The peak at 1641 cm^{-1} is generally considered to be the oxidation of the bridging nitrate peaks (NO_3^-) formed by the oxidation of adsorbed state of NO nitrate, where NO readily formed nitrate on the catalyst surface under the conditions of O_2 participation [66,67]. With the continuous passage of NH_3, the adsorption peak of nitrate at 1059 cm^{-1} rapidly disappeared and the peak intensities of nitrate located at other wave numbers did not change significantly in attenuation. The re-appearance of the associated absorption peaks of NH_3 and NH_4^+ species masked the peaks of nitrate species leaving unreacted nitrate species on the catalyst surface. The results show that the adsorbed state of NH_3 on the surface of $CeWO_x$@ZSM-5 and $CeWO_x$/ZSM-5 catalysts can react with gas-phase NO + O_2, which is consistent with the E-R mechanism. In contrast, for the L-H mechanism, adsorbed NO is oxidized to nitrate species and only a small fraction of nitrate species reacts with the adsorbed state NH_3, and the catalyst is still covered with a large amount of nitrate species, so the NH_3 -SCR reaction over $CeWO_x$@ZSM-5 and $CeWO_x$/ZSM-5 catalysts mainly follows E-R mechanism rather than L-H mechanism.

3.4.2. Reasons for K tolerance over $CeWO_x$@ZSM-5

To investigate the resistance of $CeWO_x$@ZSM-5 to alkali metals (K) compared to $CeWO_x$/ZSM-5, transient DRIFTS experiments were performed on the poisoned catalysts to measure the adsorption capacity of NH_3 and thus the toxic effect of alkali metals (K) on the acidic sites of the catalysts. As shown in Fig. 6a, b, in-situ DRIFTs were performed at 300 °C for the reactions reached adsorption saturation after 1 h of pre-adsorption by NH_3 species on 1% K-$CeWO_x$ @ZSM-5 and 1% K-$CeWO_x$/ZSM-5, all also showed similar spectral bands as described above. The deformation of NH_4^+ adsorption on protonic site and the adsorption NH_3 vibrations on the L-acid sites (1460, 1641, 1160 and 1076 cm^{-1}). The peak located at 1460 cm^{-1} was attributed to NH_4^+ adsorbed on the Brønsted site of ZSM-5. The intensity of the peaks located at 1460 cm^{-1} for 1% K-$CeWO_x$@ZSM-5 and 1% K-$CeWO_x$/ZSM-5 catalysts decreased significantly after being poisoned by K, demonstrating that the acid site of H-ZSM-5 was occupied by K. Due to the protection of the ZSM-5 shell layer, the peak intensities of NH_3 adsorption on the Lewis acid sites at 1663 cm^{-1} and 1160 cm^{-1} for the 1% K-$CeWO_x$@ZSM-5 catalysts remained well maintained, thereby maintaining the high conversion of NO_x in the NH_3-SCR reaction [68].

Combined with the above analysis, it showed that the alkali metal (K) strongly affected the ammonia adsorption on the 1% K-$CeWO_x$@ZSM-5 catalyst, and the alkali metal (K) acted on the catalyst surface to neutralize the catalyst surface acidity, which decreased the surface acidity intensity. All these results and analysis demonstrated the anti-poisoning mechanism of alkali metals on the SCR reaction over $CeWO_x$@ZSM-5 catalysts (Fig. 6c) were confirmed. Alkali metal (K) poisoning only affected the intensity of the acidic sites (NH_3 adsorption amount) and did not change the type of acid. The core-shell structure can also effectively protect the active component of the catalyst from K poisoning. This is why 1% K-$CeWO_x$@ZSM-5 showed better SCR activity than 1% K-$CeWO_x$/ZSM-5.

4. Conclusions

In summary, zeolite coupling $CeWO_x$ ($CeWO_x$@ZSM-5) catalysts with core-shell structures were prepared by a simple dry-gel conversion method and applied for NO_x reduction in this study. The as-prepared $CeWO_x$@ZSM-5 catalysts the NO_x conversion was still more than 80% within the 300–500 °C and with low concentration of N_2O by-products

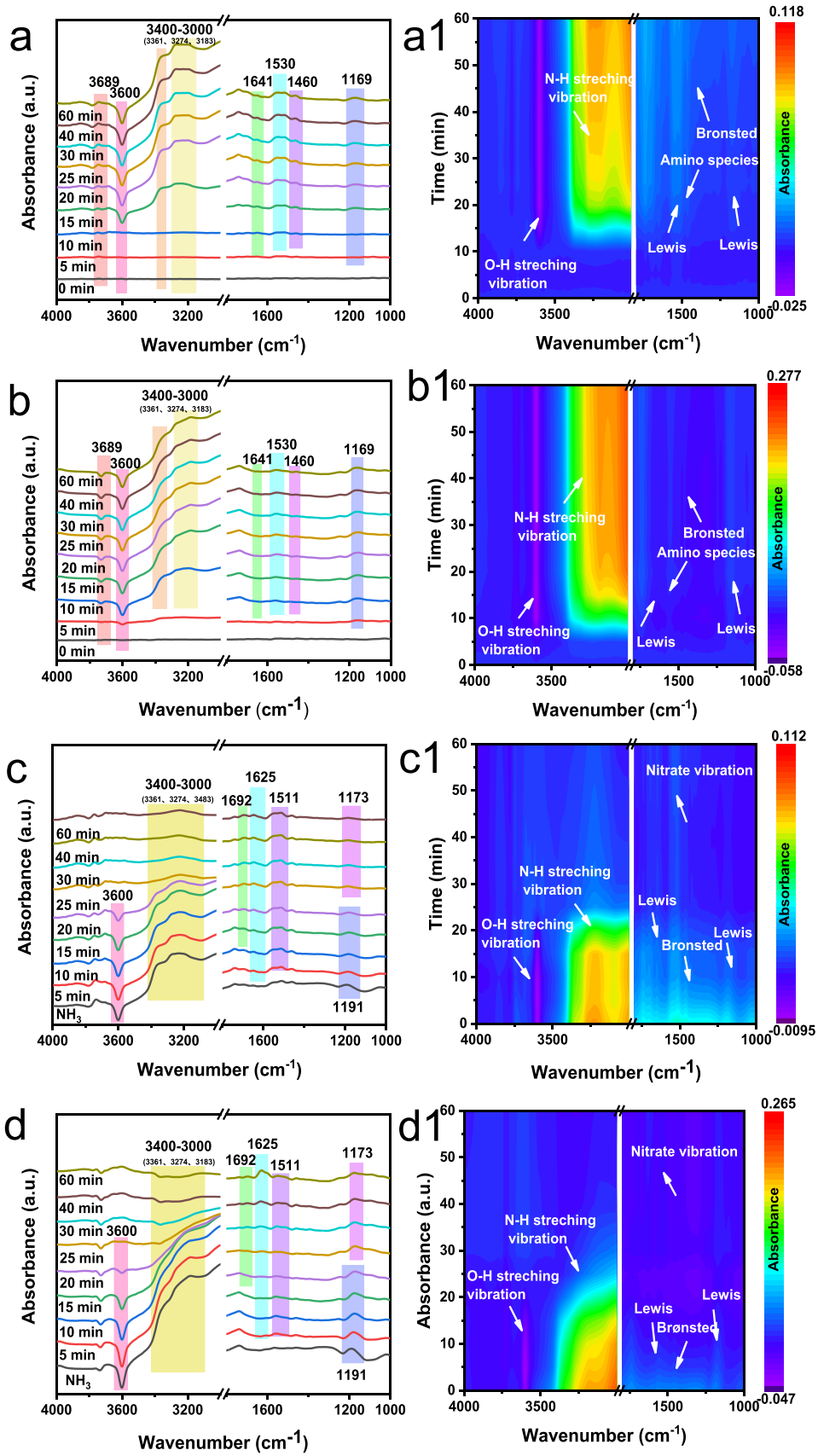

Fig. 5. The transient NH_3 adsorption DRIFTS profiles of $CeWO_x$@ZSM-5 (a) and $CeWO_x$/ZSM-5 (b) measured at 250 °C; *In situ* DRIFTS profiles of NO + O_2 reacted with the pre-adsorbed NH_3 at 250 °C of (c) $CeWO_x$@ZSM-5 and (d) $CeWO_x$/ZSM-5. The right figures are the mapping results derived from the DRITFS profiles.

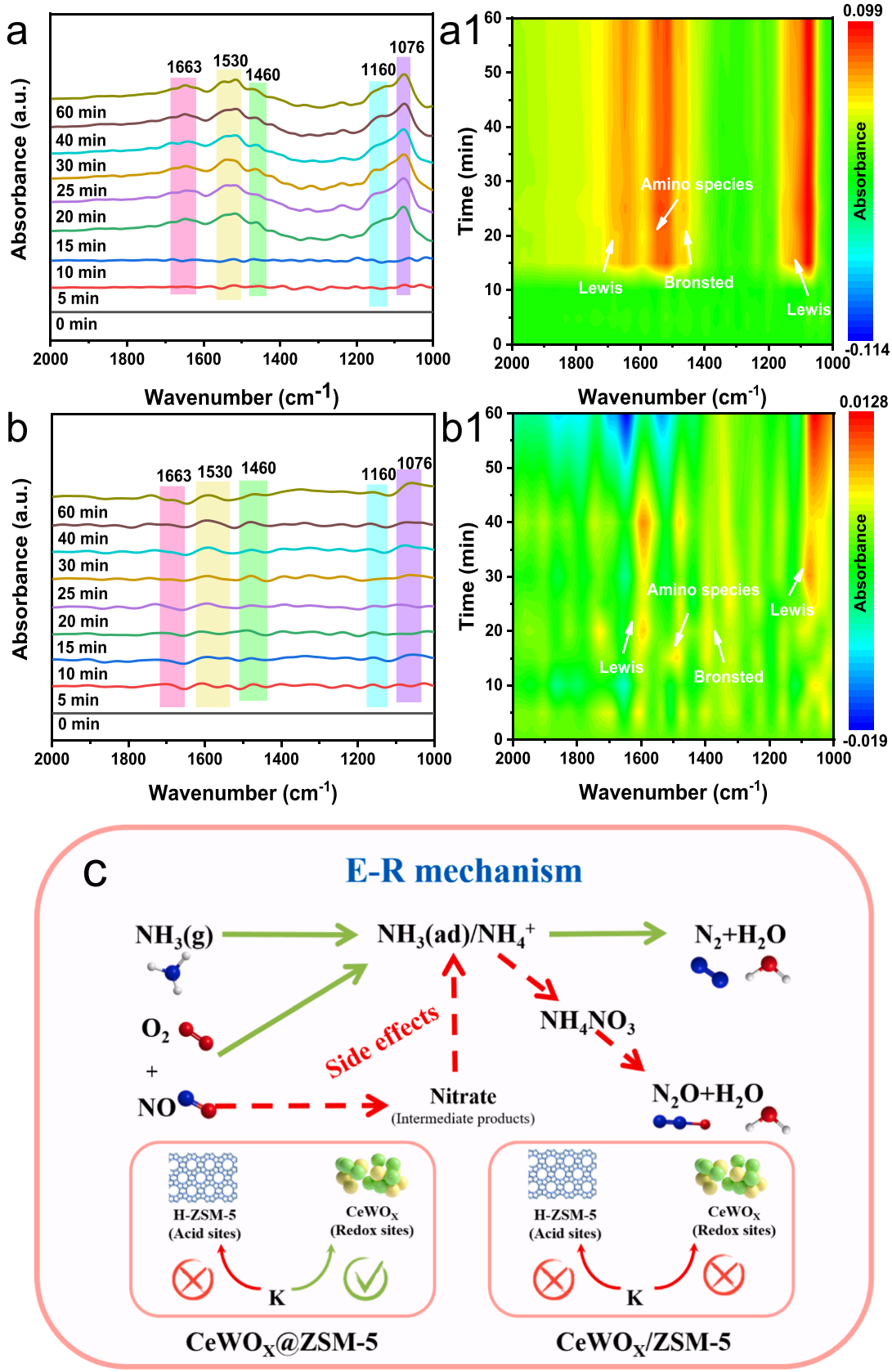

Fig. 6. The transient NH_3 adsorption DRIFTS profiles of 1% K-$CeWO_x$@ZSM-5 (a) and 1% K-$CeWO_x$/ZSM-5 (b) measured at 300 °C the right figures are the mapping results derived from the DRITFS profiles; (c) proposed NH_3-SCR reaction mechanism over $CeWO_x$@ZSM-5 and $CeWO_x$/ZSM-5.

even under high loading 1 wt% K treatment conditions. The ZSM-5 zeolite shell layer with abundant acid sites can act as a "sacrificial agent" to preferentially bind to the alkali metal (K) and prevent it from directly poisoning the active component of the catalyst, thereby decelerating catalyst deactivation after alkali poisoning. At the same time, the ZSM-5 zeolite shell layer wrapped around the Ce-W oxide species significantly improves the high-temperature hydrothermal stability of the catalyst and reduces the occurrence of high-temperature sintering. Therefore, the proposed zeolite coupling metal oxide ($CeWO_x$@ZSM-5) catalyst can mitigate the alkali metal poisoning of industrial SCR catalysts in practical reaction atmospheres. This work may serve as a guide to developing other *de*NO_x catalysts with excellent resistance to alkali metal poisoning.

CRediT authorship contribution statement

Gang Li: Methodology, Formal analysis, Data curation, Writing – original draft, Writing – review & editing, Visualization. **Yonglong Li:** Methodology, Formal analysis, Writing – review & editing. **Dong Han:** Methodology, Investigation. **Meiyuan Liao:** Methodology, Investigation. **Lei Chen:** Methodology, Investigation. **Zhenguo Li:** Methodology, Investigation. **Linsheng Wei:** Methodology, Resources. **Shengyong Lu:** Methodology, Resources. **Wenming Liu:** Methodology, Resources. **Daishe Wu:** Methodology, Resources. **Honggen Peng:** Project administration, Funding acquisition, Supervision, Writing – review & editing.

Declaration of Competing Interest

The authors declare that they have no known competing financial interests or personal relationships that could have appeared to influence the work reported in this paper.

Data availability

Data will be made available on request.

Acknowledgments

Support for this work from the National Natural Science Foundation of China (22276076 and 21976078), the Natural Science Foundation of Jiangxi Province (20202ACB213001), the National Engineering Laboratory for Mobile Source Emission Control Technology (NELMS2019A12), and the State Key Laboratory of Clean Energy Utilization (ZJUCEU2022015) is greatly acknowledged by Honggen Peng.

Appendix A. Supplementary material

Supplementary data associated with this article can be found in the online version at doi:10.1016/j.apcatb.2023.122872.

References

[1] B. Hu, C. Liu, Y. Yang, B. Wang, D. Cai, W. Xu, Adaptive internal model control of SCR denitration system based on multi-objective optimization, IEEE Access 10 (2022) 24769–24785.
[2] X. Li, Y. Ai, Y. Ge, J. Qi, Q. Feng, J. Hu, W.C. Porter, Y. Miao, H. Mao, T. Jin, Integrated effects of SCR, velocity, and air-fuel ration on gaseous pollutants and CO_2 emissions from China V and VI heavy-duty diesel vehicles, Sci. Total Environ. 811 (2022) 152311.
[3] S. Ge, X. Liu, J. Liu, H. Liu, H. Liu, X. Chen, G. Wang, J. Chen, G. Zhang, Y. Zhang, J. Li, Synthesis of Ti_xSn_1-xO_2 mixed metal oxide for copper catalysts as high-efficiency NH_3 selective catalytic oxidation, Fuel 314 (2022) 123061.
[4] Y. Guo, L. Luo, Y. Zheng, J. Wang, T. Zhu, Low-medium temperature application of selective catalytic reduction denitration in cement flue gas through a pilot plant, Chemosphere 276 (2021) 130182.
[5] B. Wang, M. Wang, L. Han, Y. Hou, W. Bao, C. Zhang, G. Feng, L. Chang, Z. Huang, J. Wang, Improved activity and SO_2 resistance by Sm-modulated redox of $MnCeSmTiO_x$ mesoporous amorphous oxides for low-temperature NH_3-SCR of NO, ACS Catal. 10 (2020) 9034–9045.
[6] W. Tan, J. Wang, Y. Cai, L. Li, S. Xie, F. Gao, F. Liu, L. Dong, Molybdenum oxide as an efficient promoter to enhance the NH_3-SCR performance of CeO_2-SiO_2 catalyst for NO removal, Catal. Today 397–399 (2022) 475–483.
[7] L. Zhu, J. Yao, G. Ma, P. Cao, S. Wu, Z. Li, NH_3-SCR performance and SO_2 resistance comparison of CeO_2 based catalysts with Fe/Mo additive surface decoration, Chem. Eng. J. 428 (2022), 131372.
[8] T. Andana, K.G. Rappé, N.C. Nelson, F. Gao, Y. Wang, Selective catalytic reduction of NO_x with NH_3 over Ce-Mn oxide and Cu-SSZ-13 composite catalysts-low temperature enhancement, Appl. Catal. B Environ. 316 (2022), 121522.
[9] S. Li, W. Huang, H. Xu, T. Chen, Y. Ke, Z. Qu, N. Yan, Alkali-induced deactivation mechanism of V_2O_5-WO_3/TiO_2 catalyst during selective catalytic reduction of NO by NH_3 in aluminum hydrate calcining flue gas, Appl. Catal. B Environ. 270 (2020), 118872.
[10] D. Wang, Q. Chen, X. Zhang, C. Gao, B. Wang, X. Huang, Y. Peng, J. Li, C. Lu, J. Crittenden, Multipollutant control (MPC) of flue gas from stationary sources using SCR technology: a critical review, Environ. Sci. Technol. 55 (2021) 2743–2766.
[11] S. Xiong, J. Chen, N. Huang, T. Yan, Y. Peng, J. Li, The poisoning mechanism of gaseous HCl on low-temperature SCR catalysts: MnO-CeO_2 as an example, Appl. Catal. B Environ. 267 (2020), 118668.
[12] X. Wang, Q. Cong, L. Chen, Y. Shi, Y. Shi, S. Li, W. Li, The alkali resistance of CuNbTi catalyst for selective reduction of NO by NH_3: a comparative investigation with VWTi catalyst, Appl. Catal. B Environ. 246 (2019) 166–179.
[13] I. Song, S.W. Jeon, H. Lee, D.H. Kim, Tailoring the mechanochemical interaction between vanadium oxides and zeolite for sulfur-resistant $DeNO_x$ catalysts, Appl. Catal. B Environ. 316 (2022), 121672.
[14] X. Du, X. Gao, R. Qu, P. Ji, Z. Luo, K. Cen, The influence of alkali metals on the Ce-Ti mixed oxide catalyst for the selective catalytic reduction of NO_x, ChemCatChem 4 (2012) 2075–2081.
[15] L. Chen, J. Li, M. Ge, The poisoning effect of alkali metals doping over nano V_2O_5-WO_3/TiO_2 catalysts on selective catalytic reduction of NO_x by NH_3, Chem. Eng. J. 170 (2011) 531–537.
[16] Y. Li, S. Cai, P. Wang, T. Yan, J. Zhang, D. Zhang, Improved NO_x reduction over phosphate-modified Fe_2O_3/TiO_2 catalysts via tailoring reaction paths by in situ creating alkali-poisoning sites, Environ. Sci. Technol. 55 (2021) 9276–9284.
[17] C. Feng, P. Wang, X. Liu, F. Wang, T. Yan, J. Zhang, G. Zhou, D. Zhang, Alkali-resistant catalytic reduction of NO_x via naturally coupling active and poisoning sites, Environ. Sci. Technol. 55 (2021) 11255–11264.
[18] D. Xu, W. Wu, P. Wang, J. Deng, T. Yan, D. Zhang, Boosting the alkali/heavy metal poisoning resistance for NO removal by using iron-titanium pillared montmorillonite catalysts, J. Hazard. Mater. 399 (2020) 122947.
[19] J. Ji, Y. Tang, L. Han, P. Ran, W. Song, Y. Cai, W. Tan, J. Sun, C. Tang, L. Dong, Cerium manganese oxides coupled with ZSM-5: a novel SCR catalyst with superior K resistance, Chem. Eng. J. 445 (2022), 136530.
[20] Y. Peng, J. Li, W. Si, X. Li, W. Shi, J. Luo, J. Fu, J. Crittenden, J. Hao, Ceria promotion on the potassium resistance of MnO_x/TiO_2 SCR catalysts: an experimental and DFT study, Chem. Eng. J. 269 (2015) 44–50.
[21] L. Zheng, M. Zhou, Z. Huang, Y. Chen, J. Gao, Z. Ma, J. Chen, X. Tang, Self-protection mechanism of hexagonal WO_3-based $DeNO_{(x)}$ catalysts against alkali poisoning, Environ. Sci. Technol. 50 (2016) 11951–11956.
[22] Z. Di, H. Wang, R. Zhang, H. Chen, Y. Wei, J. Jia, ZSM-5 core-shell structured catalyst for enhancing low-temperature NH_3-SCR efficiency and poisoning resistance, Appl. Catal. A Gen. 630 (2022), 118438.
[23] R. Yan, S. Lin, Y. Li, W. Liu, Y. Mi, C. Tang, L. Wang, P. Wu, H. Peng, Novel shielding and synergy effects of Mn-Ce oxides confined in mesoporous zeolite for low temperature selective catalytic reduction of NO_x with enhanced SO_2/H_2O tolerance, J. Hazard. Mater. 396 (2020) 122592.
[24] W. Shan, F. Liu, H. He, X. Shi, C. Zhang, Novel cerium-tungsten mixed oxide catalyst for the selective catalytic reduction of NO_x with NH_3, Chem. Commun. 47 (2011) 8046–8048.
[25] Y. Peng, J. Li, L. Chen, J. Chen, J. Han, H. Zhang, W. Han, Alkali metal poisoning of a CeO_2-WO_3 catalyst used in the selective catalytic reduction of NO_x with NH_3: an experimental and theoretical study, Environ. Sci. Technol. 46 (2012) 2864–2869.
[26] Y.J. Kim, H.J. Kwon, I. Heo, I. Nam, B.K. Cho, J.W. Choung, M. Cha, G.K. Yeo, Mn–Fe/ZSM5 as a low-temperature SCR catalyst to remove NO_x from diesel engine exhaust, Appl. Catal. B Environ. 126 (2012) 9–21.
[27] K. Guo, J. Ji, W. Song, J. Sun, C. Tang, L. Dong, Conquering ammonium bisulfate poison over low-temperature NH_3-SCR catalysts: a critical review, Appl. Catal. B Environ. 297 (2021), 120388.
[28] J. Liu, G. He, W. Shan, Y. Yu, Y. Huo, Y. Zhang, M. Wang, R. Yu, S. Liu, H. He, Introducing tin to develop ternary metal oxides with excellent hydrothermal stability for NH_3 selective catalytic reduction of NO, Appl. Catal. B Environ. 291 (2021), 120125.
[29] Y. Xi, C. Su, N.A. Ottinger, Z.G. Liu, Effects of hydrothermal aging on the sulfur poisoning of a Cu-SSZ-13 SCR catalyst, Appl. Catal. B Environ. 284 (2021), 119749.
[30] J. Park, H. Park, J. Baik, I. Nam, C. Shin, J. Lee, B. Cho, S. Oh, Hydrothermal stability of CuZSM5 catalyst in reducing NO by NH_3 for the urea selective catalytic reduction process, J. Catal. 240 (2006) 47–57.
[31] H.O. Otor, J.B. Steiner, C. Garcia-Sancho, A.C. Alba-Rubio, Encapsulation methods for control of catalyst deactivation: a review, ACS Catal. 10 (2020) 7630–7656.
[32] H. Wang, B. Huang, C. Yu, M. Lu, H. Huang, Y. Zhou, Research progress, challenges and perspectives on the sulfur and water resistance of catalysts for low temperature selective catalytic reduction of NO_x by NH_3, Appl. Catal. A Gen. 588 (2019) 117207.

[33] R. Yu, Z. Zhao, S. Huang, W. Zhang, Cu-SSZ-13 zeolite–metal oxide hybrid catalysts with enhanced SO_2-tolerance in the NH_3-SCR of NO_x, Appl. Catal. B Environ. 269 (2020), 118825.
[34] S.T. Choo, S.D. Yim, I. Nam, S. Ham, J. Lee, Effect of promoters including WO_3 and BaO on the activity and durability of V_2O_5/sulfated TiO_2 catalyst for NO reduction by NH_3, Appl. Catal. B Environ. 44 (2003) 237–252.
[35] Y. Huo, K. Liu, J. Liu, H. He, Effects of SO_2 on standard and fast SCR over $CeWO_x$: a quantitative study of the reaction pathway and active sites, Appl. Catal. B Environ. 301 (2022) 120784.
[36] A. Stahl, Z. Wang, T. Schwämmle, J. Ke, X. Li, Novel Fe-W-Ce mixed oxide for the selective catalytic reduction of NO_x with NH_3 at low temperatures, Catalysts 7 (2017) 71.
[37] R. Lin, J. Wan, Y. Xiong, K. Wu, W. Cheong, G. Zhou, D. Wang, Q. Peng, C. Chen, Y. Li, Quantitative study of charge carrier dynamics in well-defined WO_3 nanowires and nanosheets: insight into the crystal facet effect in photocatalysis, J. Am. Chem. Soc. 140 (2018) 9078–9082.
[38] D.P. DePuccio, L. Ruiz-Rodriguez, E. Rodriguez-Castellon, P. Botella, J.M. Lopez Nieto, C.C. Landry, Investigating the influence of Au nanoparticles on porous SiO_2-WO_3 and WO_3 methanol transformation, Catal. J. Phys. Chem. C 120 (2016) 27954–27963.
[39] L. Jiang, Y. Cai, M. Jin, Z. Zhu, Y. Wang, The influence of Ce or Mn doping on Cu-based catalysts for De-NO_x with NH_3-SCR, J. Chem. 2020 (2020) 1–8.
[40] C. Liu, Y. Bi, H. Wang, Z. Zhang, J. Wang, M. Guo, Q. Liu, Promotional effects on NH_3-SCR performance of CeO_2-SnO_2 catalysts doped by TiO_2: a mechanism study, Catal. Surv. Asia 25 (2021) 48–57.
[41] L. Yan, Y. Ji, P. Wang, C. Feng, L. Han, H. Li, T. Yan, L. Shi, D. Zhang, Alkali and phosphorus resistant zeolite-like catalysts for NO_x reduction by NH_3, Environ. Sci. Technol. 54 (2020) 9132–9141.
[42] L. Zhang, J. Sun, L. Li, S. Ran, G. Li, C. Li, C. Ge, L. Dong, Selective catalytic reduction of NO by NH_3 on CeO_2-MO_x (M = Ti, Si, and Al) dual composite catalysts: impact of surface acidity, Ind. Eng. Chem. Res. 57 (2018) 490–497.
[43] J. Gong, D. Wang, J. Li, N. Currier, A. Yezerets, Dynamic oxygen storage modeling in a three-way catalyst for natural gas engines: a dual-site and shrinking-core diffusion approach, Appl. Catal. B Environ. 203 (2017) 936–945.
[44] A.S. Mamede, E. Payen, P. Grange, G. Poncelet, A. Ion, M. Alifanti, et al., Characterization of WO_x/CeO_2 catalysts and their reactivity in the isomerization of hexane, J. Catal. 223 (2004) 1–12.
[45] J. Gonzalez, J.A. Wang, L.F. Chen, M.E. Manriquez, J.M. Dominguez, Structural defects, lewis acidity, and catalysis properties of mesostructured WO_3/SBA-15 nanocatalysts, J. Phys. Chem. C 121 (2017) 23988–23999.
[46] Y. Peng, K. Li, J. Li, Identification of the active sites on CeO_2-WO_3 catalysts for SCR of NO_x with NH_3: an in situ IR and Raman spectroscopy study, Appl. Catal. B Environ. 140 (2013) 483–492.
[47] R. Yu, Z. Zhao, C. Shi, W. Zhang, Insight into the synergic effect of Fe-SSZ-13 zeolite and $FeMnTiZrO_x$ catalyst with enhanced reactivity in NH_3-SCR of NO_x, J. Phys. Chem. C 123 (2019) 2216–2227.
[48] J. Ji, Y. Tang, L. Han, P. Ran, W. Song, Y. Cai, W. Tan, J. Sun, C. Tang, L. Dong, Cerium manganese oxides coupled with ZSM-5: a novel SCR catalyst with superior K resistance, Chem. Eng. J. 445 (2022), 136530.
[49] L. Yan, Y. Gu, L. Han, P. Wang, H. Li, T. Yan, S. Kuboon, L. Shi, D. Zhang, Dual promotional effects of TiO_2-decorated acid-treated MnO_x octahedral molecular sieve catalysts for alkali-resistant reduction of NO_x, ACS Appl. Mater. Interfaces 11 (2019) 11507–11517.
[50] G. Zhang, W. Han, H. Zhao, L. Zong, Z. Tang, Solvothermal synthesis of well-designed ceria-tin-titanium catalysts with enhanced catalytic performance for wide temperature NH_3-SCR reaction, Appl. Catal. B Environ. 226 (2018) 117–126.
[51] Z. Liu, S. Zhang, J. Li, J. Zhu, L. Ma, Novel V_2O_5-CeO_2/TiO_2 catalyst with low vanadium loading for the selective catalytic reduction of NO_x by NH_3, Appl. Catal. B Environ. 158 (2014) 11–19.
[52] X. Tang, Y. Shi, F. Gao, S. Zhao, H. Yi, Z. Xie, Promotional role of Mo on $Ce_{0.3}FeO_x$ catalyst towards enhanced NH_3-SCR catalytic performance and SO_2 resistance, Chem. Eng. J. 398 (2020), 125619.
[53] S. Liu, P. Yao, Q. Lin, S. Xu, M. Pei, J. Wang, H. Xu, Y. Chen, Optimizing acid promoters of Ce-based NH_3-SCR catalysts for reducing NO_x emissions, Catal. Today 382 (2021) 34–41.
[54] Q.A. Drmosh, Y.A. Al Wajih, R. Al-Rammah, M. Qamar, Z.H. Yamani, Surface-engineered WO_3 thin films for efficient NO_2 sensing, Appl. Surf. Sci. 517 (2020) 146235.
[55] H. Xu, J. Liu, Z. Zhang, S. Liu, Q. Lin, Y. Wang, S. Dai, Y. Chen, Design and synthesis of highly-dispersed WO_3 catalyst with highly effective NH_3-SCR activity for NO_x abatement, ACS Catal. 9 (2019) 11557–11562.
[56] W. Tan, A. Liu, S. Xie, Y. Yan, T.E. Shaw, Y. Pu, K. Guo, L. Li, S. Yu, F. Gao, F. Liu, L. Dong, Ce-Si mixed oxide: a high sulfur resistant catalyst in the NH_3-SCR reaction through the mechanism-enhanced process, Environ. Sci. Technol. 55 (2021) 4017–4026.
[57] W. Liu, Z. Gao, X. Zhao, J. Gao, R. Yang, L. Yu, Promotion effect of chromium on the activity and SO_2 resistance of CeO_2-TiO_2 catalysts for the NH_3-SCR reaction, Ind. Eng. Chem. Res. 60 (2021) 11676–11688.
[58] Z. Lian, W. Shan, Y. Zhang, M. Wang, H. He, Morphology-dependent catalytic performance of NbO_x/CeO_2 catalysts for selective catalytic reduction of NO_x with NH_3, Ind. Eng. Chem. Res. 57 (2018) 12736–12741.
[59] Z. Liu, S. Zhang, J. Li, L. Ma, Promoting effect of MoO_3 on the NO_x reduction by NH_3 over CeO_2/TiO_2 catalyst studied with in situ DRIFTS, Appl. Catal. B Environ. 144 (2014) 90–95.
[60] L. Yan, Y. Ji, P. Wang, C. Feng, L. Han, H. Li, T. Yan, L. Shi, D. Zhang, Alkali and phosphorus resistant zeolite-like catalysts for NO_x reduction by NH_3, Environ. Sci. Technol. 54 (2020) 9132–9141.
[61] H. Xue, X. Guo, T. Meng, Q. Guo, D. Mao, S. Wang, Cu-ZSM-5 catalyst impregnated with Mn-Co oxide for the selected catalytic reduction of NO: physicochemical property-catalytic activity relationship and in situ DRIFTS study for the reaction mechanism, ACS Catal. 11 (2021) 7702–7718.
[62] T. Zhang, J. Shi, J. Liu, D. Wang, Z. Zhao, K. Cheng, J. Li, Enhanced hydrothermal stability of Cu-ZSM-5 catalyst via surface modification in the selective catalytic reduction of NO with NH_3, Appl. Surf. Sci. 375 (2016) 186–195.
[63] S. Zhan, M. Qiu, S. Yang, D. Zhu, H. Yu, Y. Li, Facile preparation of MnO_2 doped Fe_2O_3 hollow nanofibers for low temperature SCR of NO with NH_3, J. Mater. Chem. A 2 (2014) 20486–20493.
[64] L. Chen, J. Li, M. Ge, DRIFT study on cerium-tungsten/titiania catalyst for selective catalytic reduction of NO_x with NH_3, Environ. Sci. Technol. 44 (2010) 9590–9596.
[65] D. Meng, W. Zhan, Y. Guo, Y. Guo, L. Wang, G. Lu, A highly effective catalyst of Sm-MnO_x for the NH_3-SCR of NO_x at low temperature: promotional role of Sm and its catalytic performance, ACS Catal. 5 (2015) 5973–5983.
[66] B. Liu, J. Liu, S. Ma, Z. Zhao, Y. Chen, X. Gong, W. Song, A. Duan, G. Jiang, Mechanistic study of selective catalytic reduction of NO with NH_3 on W-doped CeO_2 catalysts: unraveling the catalytic cycle and the role of oxygen vacancy, J. Phys. Chem. C 120 (2016) 2271–2283.
[67] Z. Fan, J. Shi, C. Gao, G. Gao, B. Wang, Y. Wang, C. He, C. Niu, Gd-modified MnO_x for the selective catalytic reduction of NO by NH_3: the promoting effect of Gd on the catalytic performance and sulfur resistance, Chem. Eng. J. 348 (2018) 820–830.
[68] Z. Shen, X. Liu, S. Impeng, C. Zhang, T. Yan, P. Wang, D. Zhang, Alkali and heavy metal copoisoning resistant catalytic reduction of NO_x via liberating lewis acid sites, Environ. Sci. Technol. 56 (2022) 5141–5149.